Transfer Operator Based Approach for Optimal Sensor Placement Under Uncertain Operating Conditions

Himanshu Sharma[1], Anthony D. Fontanini[2], Umesh Vaidya[3],Baskar Ganapathysubramanian[1]
[1]Department of Mechanical Engineering,Iowa State University,Ames,IA,50010,USA
[2]Fraunhofer CSE, Boston, MA 02210, USA
[3]Department of Electrical and Computer Engineering, Iowa State University,Ames,IA,50010,USA

Abstract

Sensors are an integral part of buildings to sense pollutants, identifying extreme events and for maintaining comfort. Traditionally, identification of the sensor locations is via solution of inverse problem (computationally intensive) or using some standard thumb rules which might not be suitable for every building. In recent years,the concepts of non-linear control theory is integrated with fluid dynamics to develop Perron-Frobenious(PF) operator based approaches to design sensor placement strategies. This approach alleviates the shortcomings of the previous approaches. The current paper extends the PF framework to account for uncertainty of airflow in the building to compute more robust sensor location maps. The developed approach is demonstrated for a IEA-2D benchmark problem. The algorithm is easily extensible to the complex buildings and can account for various uncertainties.

Introduction

Impurity and contaminant detection sensors have become an integral part of buildings HVAC systems. The optimal placement of these sensors in the indoor built environment is important to ensure comfort, health, as well as energy efficiency. The studies by (Sarigiannis, 2013) have shown that millions of people approximately spend 90% of time indoors. While indoor, occupants can be subjected to various air pollutants, the exposure of these pollutants are linked to various respiratory diseases (Tham, 2016), cancer (Herbstman et al., 2015) , and in extreme cases loss of life (Baur et al., 1993). The transmission of the infectious diseases (TID) (like influenza, tuberculosis, smallpox, chickenpox, and SARS) has been widely studied by various authors (Olsen et al., 2003; Namilae et al., 2017; Wenzel, 1996; Kenyon et al., 1996; Duong and Waldman, 2016; Li et al., 2016; Buhr et al., 2016; Kawashima et al., 2016) to understand the connection between diseases and air transport. The spread of TID is also discussed in detail by (Tham, 2016). Further,the threats of using chemical and biological warfare (CBW) for terror and mass destruction has also lead researchers for developing methods and response strategies to avoid these dangerous events (Stuart and Wilkening, 2005; Ostfield et al., 2004; Demirev et al., 2005). The use of CBW agents might not be likely, but a single attack can be devastating. Fast detection, containment, and response to the release of CBW agent is essential to reduce the casualties and execute an evacuation plan.
In a general sense, addressing the issues of TID, CBW and IAQ problems involves performing risk assessments, implementing preventive measures, recognizing problem areas, identifying potential sources, and designing evacuation strategies (Fontanini et al., 2016). Sensor locations are an integral part for all of these steps. Sensors also play an important role for feedback in the control of HVAC systems. Researchers have also shown that energy savings can be improved by optimal sensor response and can also efficiently help in maintaining IAQ of the building (Du et al., 2015; Lu et al., 2011; Chao and Hu, 2004; Fisk and De Almeida, 1998). Sensor placement design with the development of wireless network (Zhou et al., 2015) has eased the process for data collection and integration with feedback systems to control the mechanical system. Therefore, an optimal sensor placement for a building is not only important for reducing the risk of infections but also for making buildings more energy efficient. Furthermore, prompt response to a release of a CBW agent requires sensor locations that minimizes the time between the release and the detection of the threat.
To obtain the optimal location of sensors, solution methods for sensor placement are generally classified in two categories: 1) engineering/heuristic methods; 2) optimization methods and/or inverse methods. Both these approaches have been widely studied in the buildings community. While the former approach is fast, challenges of this approach include the lack of a formal methodology to rationally design response time, ensuring full/partial coverage of the indoor environment, and challenges to generalizing the approach for multiple rooms or zones (Liu and Zhai, 2009b) and accounting for uncertainty in the flow field. This has resulted in the increased popularity of the latter approach (Liu and Zhai, 2009a; Mazumdar and Chen, 2008; Zhang and Chen, 2007; Chen and Wen, 2008; Zhou and Haghighat, 2009). However, most current optimization/inverse approaches have their own challenges that preclude widespread

usage. These challenges include the computational complexity of solving partial differential equations, as well as the specificity of the results to precise release scenarios.

In this context, there has been some recent work that seeks to integrate control theory concepts into contaminant transport via the use of the Perron-Frobenius (PF) operator (Rajaram et al., 2010; Fontanini et al., 2016). The discrete form of the PF operator, which takes the form of the Markov matrix, has been used predict particle transport in enclosed environment by (Chen et al., 2015a,b; Fontanini et al., 2015, 2017). This PF operator based mathematical approach dramatically simplifies the optimization problem by converting a flow field (which can be either experimentally determined or computationally modelled) into a Markov matrix.

A Markov based approach converts the problem of solving partial differential equations to model contaminant transport into a problem computing simple matrix-vector products. Prior developments have been focused on a single steady state or time-varying flow field scenarios. However, buildings operate at many different conditions through the year, some of these operating conditions are more likely than others, and the movement of people in the building can produce added complexity to the flow physics. All these factors affect the transport characteristics of contaminants and hence the optimal location of a sensor.

The purpose of this paper is to introduce a sensor placement algorithm that takes into account the natural stocasticity of the indoor environment. The algorithm, building upon previous work (Rajaram et al., 2010; Fontanini et al., 2016), is extended to account for the uncertain flow and operating conditions encountered in the built environment. The sensors locations are based on the *expected sensing volume* a sensor can cover. The algorithm is showcased using a flow field based on the IEA-Annex 20 (Nielsen et al., 1990) problem with multiple possible locations of a person in the room. The results from this extension will provide a more robust sensor map for a building experiencing uncertain operating conditions.

Methodology

Contaminant transport is modelled by an advection-diffusion partial differential equations (PDE) given in Eq.1. The scalar contaminant is propagated on the given airflow field, U. The flow field can be generated experimentally, as well as computationally using computational fluid dynamics (CFD).

$$\frac{\partial \Phi}{\partial t} + \nabla(U\Phi) + \nabla^2(D\Phi) = S_\Phi \qquad (1)$$

Where Φ is the scalar contaminant, D is the diffusion constant and S_Φ is the source term in eq.1. The velocity flow field U can be steady or can be a function of time.

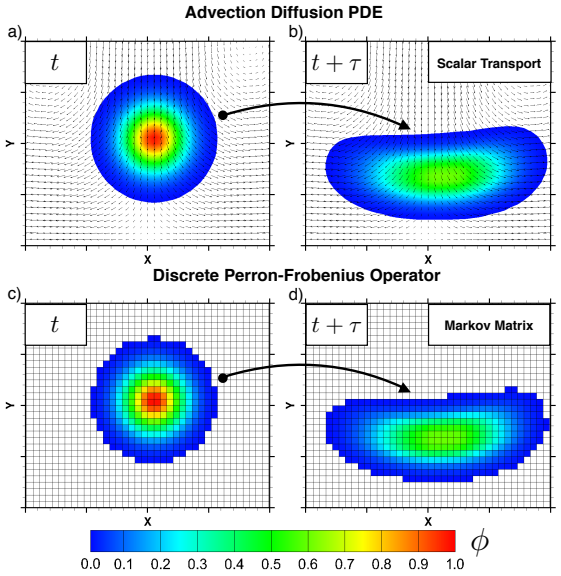

Figure 1: For the given velocity field (a)-(b)Shows the contaminant transport using the scalar transport advection diffusion equation-1(c)-(d)Shows the discrete PF-operator based scalar transport (Fontanini et al., 2016)

.

PF-operator based sensor placement: *Under Deterministic Condition*

The PDE shown in eq.1 can be observed as an operator transporting contaminant from time t to $t + \delta t$. This can be considered as an operator on Φ (Vaidya et al., 2012a; Fontanini et al., 2015, 2016). This operator is called Perron Frobenius (PF) operator $L(\cdot)$ eq.2.The discrete form of this operator is called the Markov matrix.

$$\Phi_{t+\delta t} = L(\Phi_t) \qquad (2)$$

The Markov matrix is a square matrix ($P \in \mathcal{R}^{n\times n}$) with all non-negative entries.To calculate the entries of the Markov matrix for contaminant transport, there are various methods suggested by (Chen et al., 2015b; Fontanini et al., 2015, 2017). Any of the methods discussed in these work can be used for sensor placement as long as the method captures the transport characteristics of the scalar needing to be sensed. For flexibility in choosing the sampling rate of the sensor(s), we use the Eulerian based method developed in Fontanini et al. (2017), as the Markov time step is not a limitation for this method like the other methods of (Chen et al., 2015b) and (Fontanini et al., 2015).

Once constructed the Markov matrix can be used to propagate the scalar at discrete time instances, t_i, to reach the final simulation time $t_f = t + m\delta t$. This propagation is performed by simple matrix-vector multiplication, eq.3.

$$\phi_{t_{i+1}} = \phi_{t_i} P + \hat{S}_{t_i,t_{i+1}} \quad i \in \{0,\ldots,m\} \qquad (3)$$

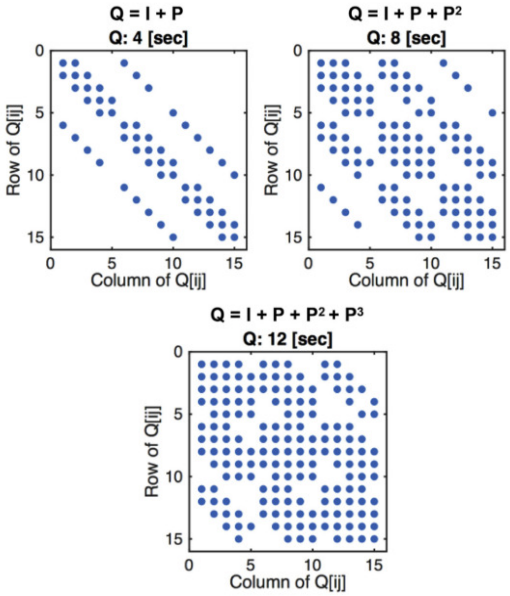

Figure 2: The contaminant tracking matrix calculated from eq.4 for 4,8 and 12 sec of an aircraft cabin Chen et al. (2014)

The source term, $\hat{S}_{t_i,t_{i+1}}$, includes volumetric and inlet sources in the domain (Fontanini et al., 2017). For the given velocity field an example demonstrating the use of this operator is shown in Fig.1. The next step after constructing the P matrix is to calculate the contaminant tracking matrix $\mathbf{Q}_\tau$.

Calculation of Contaminant Tracking Matrix

The calculation process of the volume coverage matrix begins with the calculation of the contaminant tracking matrix, $\mathbf{Q}_\tau$ Fontanini et al. (2016). Each row of the contaminant tracking matrix encodes information about the transport history of a constant contaminant source at one cell (i.e one row) for the response time of the sensor. In case of steady state flow field the contaminant tracking matrix is given by eq.4.

$$\mathbf{Q}_\tau = I + P + P^2 + \cdots + P^m \tag{4}$$

Since $P^m (= P \times P \times \cdots \times P$ m times) is the m^{th} multistep transition matrix, the contaminant tracking matrix builds a history as to where the contaminant will be propagated in m Markov time-steps. Figure 2 shows a graphical example of this process.
After the contaminant tracking matrix is obtained the sensor locations are decided in the building.

Placement of Sensors:

The release locations of the contaminant in the domain can be any state of the Markov matrix P. Therefore, the sensor locations should be chosen such that maximum number of number of states can be observed for any given release scenario. This is discussed in detail by (Fontanini et al., 2016). The approach taken by the authors is to pose the problem as a *set cover problem* of combinatorics. This essentially identifies a set of locations that maximize the coverage of states. The *greedy algorithm* presented by (Chvatal, 1979) is used to find the sensor locations according to the maximum number of covered states (Vaidya et al., 2012b).
In the simulations environment any sensor can be placed anywhere in the domain. But in real situation there are various constraints associated with the sensor placements. These real scenarios needs to be accounted in the algorithm and are discussed briefly next.

Applying Constraint & Threshold Contaminant Tracking Matrix

Each sensor has an associated measurement accuracy threshold. The accuracy threshold is dependent on the quality of the sensor. The accuracy threshold can be accounted by inspecting the column entries of the contaminant transport matrix. The column with the larger values represent a strong signal. The objective of this step is to replace those entries from the contaminant transport matrix which are below the accuracy threshold. The threshold value is a non-dimensional value that describes the ratio of value detected to the source release rate S_{source},the release time (sensing/response time) τ, $\epsilon_{acc} = \frac{\mu_{detect}}{S_{source}\tau} = \frac{\mu_{detect}}{\mu_{source}}$. The values ϵ_{acc} are usually prescribed by the sensor manufacturer. Since we have constructed a set $\mathbf{Q}_\tau$ we can apply this thresholding on the set as eq.5.

$$\mathbf{Q}^*_\tau = \mathbf{Q}_\tau > \epsilon_{acc} \tag{5}$$

This equation serves as an operator that converts a matrix with real entries, $\mathbf{Q}_\tau$, to a matrix with binary entries, $\mathbf{Q}^*_\tau$. The entries in $\mathbf{Q}^*_\tau$ that are 1 correspond to the states that can be sensed by the sensor with the accuracy of ϵ_{acc} if a sensor is located in the column in which the entry resides.
Further, not every location in a building/room are suitable to place the sensor due to practical reasons such as aesthetics, sensor installation limitations, they can also not be placed in occupied zone where occupants can affect the operation by stepping over them.
The overview for the deterministic case can be understood from the flow diagram shown in fig.3, where one starts with the given flow field U, then constructs the discrete transition map P. The map is propagated till $\tau = m\delta t$ to construct the contaminant tracking history $\mathbf{Q}_\tau$ which is then thresholded to generate the $\mathbf{Q}^*_\tau$ on which the set cover algorithm is applied.

PF-operator based sensor placement: *Uncertain Conditions*

Up to this point we have only considered a deterministic flow field inside the building. The building in general can be subjected to various weather scenarios, HVAC conditions,interior arrangements and

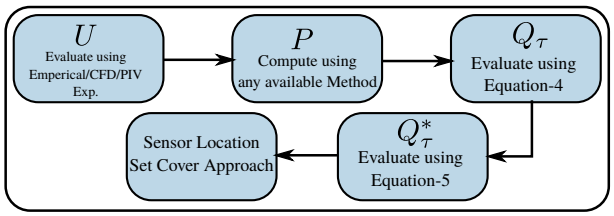

Figure 3: The flow chart for obtaining the sensor locations under deterministic flow field.

occupancies conditions. These changes brings uncertainty in the velocity field (airflow) inside the building. Considering the sensor locations obtained by only a single velocity field will not result in the optimum performance of the sensor. Therefore, it is important to account for all the velocity realizations that can occur to construct the sensor location map which can perform optimally in every flow condition. In the current study we have taken different occupancy location to demonstrate the uncertain flow fields inside the building. Occupancy is a significant factor affecting the flow field and the internal loads. The flow field is effected by the thermal plume that extends above people in the space (Salmanzadeh et al., 2012; Zukowska et al., 2012). The internal loads (the use of HVAC equipment, lighting, and electronics in the space) are effected by the presence of people and their usage of electronics in the space (Azar and Menassa, 2012).

Mathematically, we can consider these uncertain velocity flow field as belonging to a stochastic space Ω which can be written as eq.6.

$$\begin{aligned} \mathbb{U}(\bar{\mathbf{x}}, t, \chi), \text{Where, } \bar{\mathbf{x}} \in \{x, y, z\}, \\ \chi \in \Omega, t \in [0, T_f] \\ \mathbf{U} = \{U_1, \ldots, U_M\} \\ \Theta = \{\theta_1, \ldots, \theta_M\} \end{aligned} \tag{6}$$

Without loss of generality, a building can have a finite set of flow realizations belonging to this stochastic space $\mathbb{U}$ and can be expressed as a set $\mathbf{U}$. Each realization in this space has a corresponding probability set Θ associated with it Eq.6. These probabilities can be obtained via Bayesian analysis or by the occupancy scheduling of the building (Petzold et al., 2005).

Now, for placing the sensors we apply the expectation operator for each step of the deterministic flow chart shown in fig.3. Hence, the set-cover algorithm is applied on to the expected $\langle Q^*_\tau \rangle \big(= \sum_{i=1}^{M} \theta_i \widetilde{Q^*_{\tau,i}} \big)$. Before calculating these expected quantities the major challenge associated with this expectation operator calculations is, unequal dimensions of the transition matrices for each realization. For M set of velocity fields a set of transition matrices can be constructed as $\{P_1, \ldots, P_M\}$. Since, the number of states in the transition matrix $P \in \mathbf{R}^{n \times n}$ is equal to the number of cells(n) in the discretization (Fontanini et al., 2017)

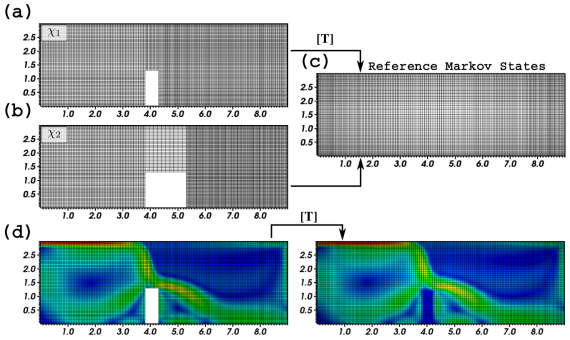

Figure 4: (a)-(b) Two original Markov states realizations with an obstruction in the domain.(c) The reference Markov states which are used for constructing the set $\widetilde{\mathbf{P}}$ (d) The velocity field of obstruction case which is mapped on to the reference state case using mapping matrix $[T]$

each P will have different dimensions. For example, fig.4(a) which represent χ_1 realization has $(p \times q)$ number of states and fig.4(b) χ_2 has $(l \times b)$ due to the different kinds of obstructions. Therefore, the expectation operator cannot be applied directly with such realizations.

To resolve this issue an additional step is performed by choosing a reference Markov discretization fig.4(c) with fixed number of states the other uncertain flow fields $\mathbb{U}$ are mapped onto the reference state. An example for a realization with an obstruction present is shown in the fig.4(d), where we map the velocity field of the obstruction states onto the reference states. We ensure that the cells in the obstruction region have zero velocity as shown in fig.4(d). The mapping results in the set $\widetilde{\mathbf{U}} = \{\widetilde{U}_1, \ldots, \widetilde{U}_M\}$ on the reference grid and then the set $\widetilde{\mathbf{P}} = \{\widetilde{P}_1, \ldots, \widetilde{P}_M\}$ is constructed. For $\widetilde{P}_M$ the contaminant tracking history is generated to construct the set of of contaminant tracking matrices $\{\mathbf{Q}_\tau = Q_{\tau,1}, \ldots, Q_{\tau,M}\}$. The thresholding is done on $\mathbf{Q}_\tau$ similarly as the deterministic case eq.5 to result in $\widetilde{\mathbf{Q}^*_\tau} = \{\widetilde{Q^*_{\tau,1}}, \ldots, \widetilde{Q^*_{\tau,M}}\}$.

In case of non-uniform discretized states shown in fig.4,the step before finding the sensor location is to calculate volumetric coverages for each flow realization. This is achieved from the constructed $\widetilde{\mathbf{Q}^*_\tau}$ multiplying by $\mathbf{V}$, as $(\widetilde{\mathbf{Q}^*_\tau} \cdot \mathbf{V})$. $\mathbf{V}$ is a diagonal matrix with the diagonal containing the normalized cell volumes, $V_{i,i} = V_{\omega_i}/V_{tot}$. In case of the uniform grid the V is equal to an identity matrix,($\mathbf{I}$). The result of this operation can be represented as set,$\widetilde{\mathbf{Q}^{**}}$ Eq.7.

$$\widetilde{\mathbf{Q}^{**}} = \{\widetilde{Q^*_{\tau,i}} \cdot \mathbf{V}\}, \quad i \in \{1, \ldots, M\} \tag{7}$$

The set $\widetilde{\mathbf{Q}^{**}}$ will be used to find the location of the sensors in an expectation sense. The set $\widetilde{\mathbf{Q}^{**}}$ shown in eq.7 is applied with L_o operator which sum over the all columns $(:, j)$ of each $\widetilde{\mathbf{Q}^{**}}_i$. The result of this operations generate another a set eq.8

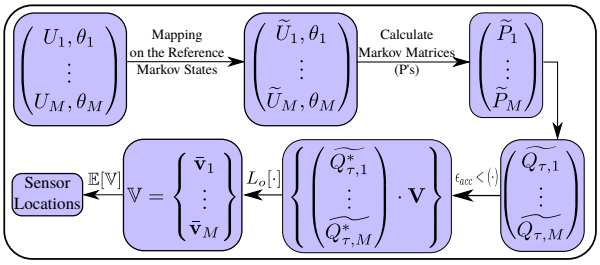

Figure 5: The flow chart of the sensor placement algorithm to account for the uncertain flow fields inside the buildings.

$\mathbb{V} = \{\bar{\mathbf{v}}_1, \ldots, \bar{\mathbf{v}}_M\}$, $\bar{\mathbf{v}}_M$, where each element vector ($\bar{\mathbf{v}}$) is of size $n \times 1$ with, n being the number of states/-cells in the domain.

$$\begin{aligned} \mathbb{V} = L_o\{\widetilde{\mathbf{Q}^{**}}\} \quad i = 1, \ldots, M \\ L_o = \sum_{(:,j)} (\widetilde{\mathbf{Q}^{**}})_i \end{aligned} \tag{8}$$

Now, the ***expectation coverage*** is evaluated by associating with each $\bar{\mathbf{v}}_M$ by there associated probabilities θ_M. The expected $\mathbb{E}[\bar{\mathbb{V}}]$ is obtained using eq.9a. The location of the first sensor is decided by finding the index where expected $\mathbb{E}[\mathbb{V}]$ is maximum using eq.9b. To find the next sensor, the information of the first sensor is removed from consideration. This is done by making corresponding $\bar{k}(\cdot)$ to zero for each $(\widetilde{\mathbf{Q}^{**}})_i$ and Eq.8-9b are repeated till all the sensors are placed in the domain.

$$\mathbb{E}[\mathbb{V}] = \sum_{i=1}^{M} \Theta_i \bar{\mathbf{v}}_i \tag{9a}$$

$$\bar{k}(1) = max(\mathbb{E}[\bar{\mathbb{V}}]) \tag{9b}$$

The overview of the complete expectation based algorithm is explained in the flow chart shown in fig-5. The given set of velocity fields and associated probabilities are mapped onto the reference Markov states. The mapped fields are then used to construct the transitions maps of each case. The maps are then used to construct the contaminant tracking history for each realization for a fixed time horizon(τ). In the next step the operational scenarios are accounted in the problem by applying sensor accuracy thresholding and constraints. In case of a non-uniform discretization each state is weighted by its volume. In the next step,the column supports for each element in the set is computed to result in a vector $\mathbb{V}$. The expectation operator is applied onto this vector space with the associated probability and then the sensor locations calculated by finding the index of the maximum entry in the expected vector. In the next sections the results obtained after applying this algorithm will be discussed in detail.

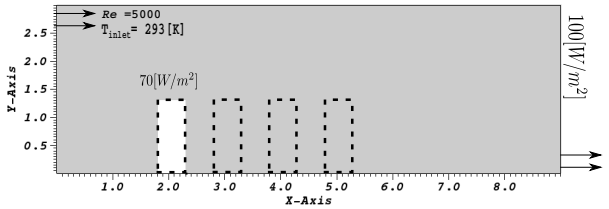

Figure 6: The boundary conditions used for four cases are shown, where the dashed line represents different locations of the person in the room.

Results and Discussion

The section presents the sensor placement results for the IEA-2D (Nielsen et al., 1990) building which is widely used by the community for benchmarking. To account for uncertain flow fields in the building four different obstruction in the room are considered (with a heated wall see fig.6). A Reynolds number of 5000 is used with RNG-K-ϵ for all the cases. The inlet temperature is set as 293 K and the obstruction representing a person is set as heat source generating 70 W/m^2. The heated wall in all the case is maintained at 100 W/m^2 while the other boundaries have the adiabatic boundary conditions. The velocity flow fields were computed for the four cases using the finite volume based open source code OpenFOAM (Jasak et al., 2007). Figure-7 shows the flow field for all the realizations. The simulations were run for a convergence tolerance of 10^{-5} and a rigorous validation of solvers were carried for non-isothermal cases by comparing experiments and numerical results. The generated flow fields were then used by the Markov matrix generation frame work to generate the contaminant transition map for each case. The transition maps were then validated to ascertain the accuracy of scalar transport discussed in following section.

Validation of Contaminant Transport by Transition/Markov Matrix

The individual transition matrix P for each flow field is constructed as discussed in the deterministic approach section. It is then used to transport the contaminant Φ. The applicability of the transition matrix based method can be tested against PDE based scalar transport. The validations are carried for the all the transition maps generated for four realisations considered in this study. The results are shown here for a single case with an obstruction where the scalar is initialized covering half of the building. Figure-8(a)show the initialized scalar map where red represents the scalar concentration as one and blue corresponds to zero. The scalar transport PDE equation is solved for final time of 50 sec using OpenFoam solver, and compared with the Markov approach. Figure-8(a-b) compares the scalar concentration contours after 50 sec by PDE and Markov approach. It can be seen that they closely match each other. The concentration profiles are also plotted and compared about

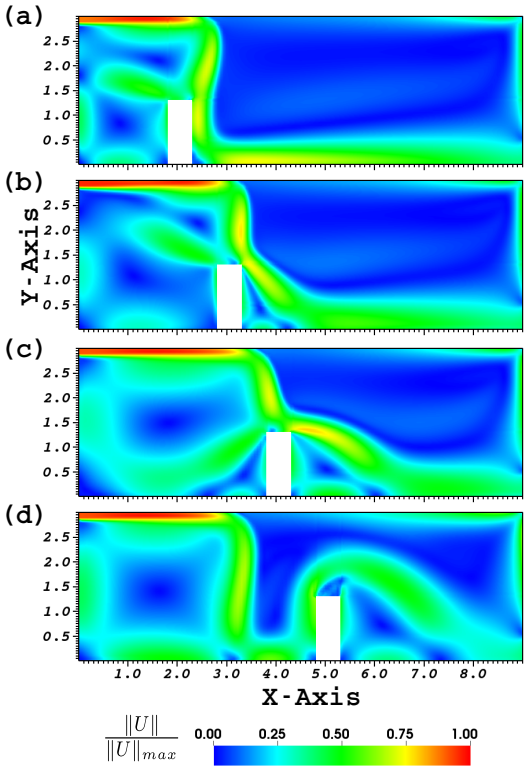

Figure 7: The flow fields U generated using CFD simulations for the obstacles at different location, notice the large variety in the flow features.

the mid-planes of the building which is shown in fig.9. The Markov results are represented as dots, which closely matches the PDE based predictions with and L_2 error of about 10^{-4}. The validations shows the accuracy of the Markov approach and effectiveness of the matrix-vector product based approach in predicting a scalar concentrations.

No Constraint Sensor Placement

In the current paper we demonstrate the developed algorithm for placing a sensor for a IEA-2D (Nielsen et al., 1990) building with no-constraint on the sensor placements. The response time and the number of sensors were 80 sec and 1 respectively, with the accuracy threshold of $\epsilon_{acc} = 0.01\%$ as used in eq.7 and $\Theta_i = 0.25$. The sensor location is obtained using the proposed algorithm. The volume coverages are shown as contours in the fig.10, the color represents the volumes sensed by the sensor. The location of the sensor is obtained using the expectation based algorithm and provide the coverage of 93.69% in expected sense. It can also be seen for each cases that the obstruction locations are not involved as the sensing regions. To represent the cumulative coverage for the study the coverages were weighted by there associative Θ_i to produce the expectation coverage map contour $\mathcal{P}$ which is shown in the fig.11, in the contour the lighter color represents the overlapped volume region regions for the computed sensor location. In the previous work of (Fontanini et al., 2016) it was shown

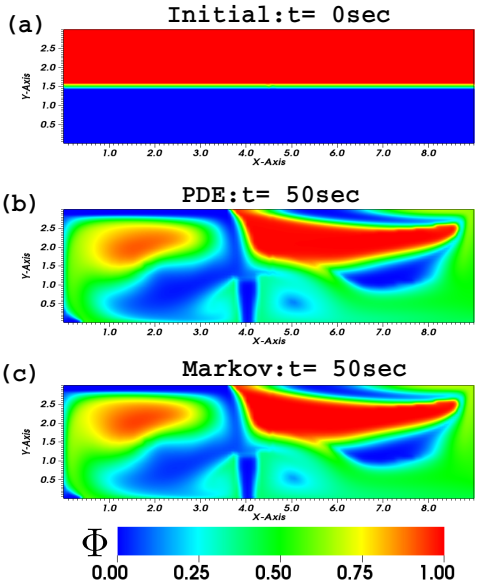

Figure 8: Comparison of the scalar Φ transport using the PDE scalar advection equation 1 and by Markov matrix.

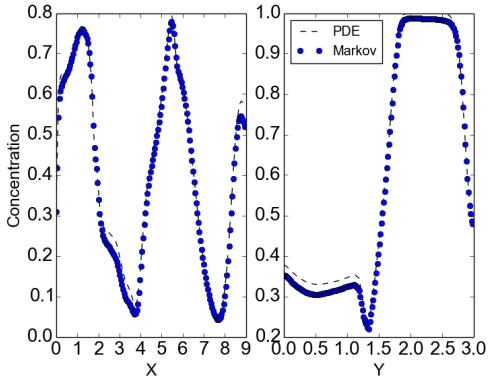

Figure 9: The scalar Φ concentration profiles along the mid X and Y planes of the building.

that in the unconstrained situations with the long time horizon the sensors are usually to be placed close to the outlet. A similar observation is also made in the present study. This can be explained as the contaminant transport is driven towards the outlet even after been dispersed for the longer period of time (80 sec), therefore outlet location is selected by the the algorithm.

Conclusion

The current work presents the extension of the PF-based approach for finding the optimal sensor placement under uncertain flow conditions. The uncertainty of the airflow inside building is considered by accounting occupancy of the building. The method is demonstrated for the IEA benchmark of the 2D building with a person at different locations in the building. The work lays the foundation for extending the approach to more complex 3-D problems and incorporating various sensors placement constraints to

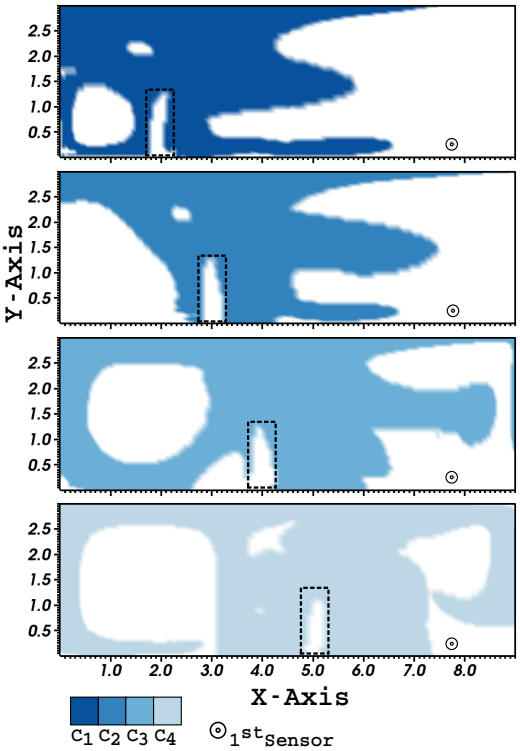

Figure 10: The individual coverages for the computed sensor location where the color represents the coverage by the sensor location.

the sensor placement. The developed algorithm also showcased an efficient way of accounting for uncertain flow fields and computing the robust sensor location map for the building. The stochastic approach developed in work allows the handling of various uncertain scenarios which can occur inside the building. As an extension the developed method can also be integrated in designing HVAC control,evacuation strategies and finding the effective sensor map for the building. As the method accounts for the sensor accuracy, therefore an interplay between the quality of different sensor can also be easily studied with the current approach. In future the method will be shown for more

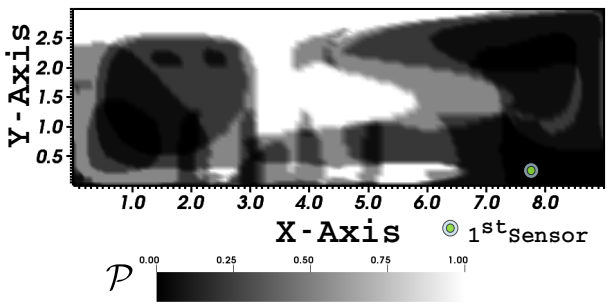

Figure 11: The Probabilistic coverages map of the sensor locations obtained by combining the individuals coverages according to the associated occupancy Θ *of individual cases.*

complex shapes by incorporating uncertainty arising due to different weather conditions, interior arrangement and constraints on the sensor placements.

Acknowledgement

The authors would like to acknowledge support from NSF 1149365 and NSF 1345381.

References

Azar, E. and C. C. Menassa (2012). A comprehensive analysis of the impact of occupancy parameters in energy simulation of office buildings. *Energy and Buildings 55*, 841–853.

Baur, X., J. Ammon, Z. Chen, A. Czuppon, and U. Beckmann (1993). Health risk in hospitals through airborne allergens for patients presensitised to latex. *The Lancet 342*(8880), 1148–1149.

Buhr, T., A. Young, M. Bensman, Z. Minter, N. Kennihan, C. Johnson, M. Bohmke, E. Borgers-Klonkowski, E. Osborn, S. Avila, A. Theys, and P. Jackson (2016, apr). Hot, humid air decontamination of a C-130 aircraft contaminated with spores of two acrystalliferous Bacillus thuringiensis strains, surrogates for Bacillus anthracis. *Journal of Applied Microbiology 120*(4), 1074–1084.

Chao, C. and J. Hu (2004). Development of a dual-mode demand control ventilation strategy for indoor air quality control and energy saving. *Building and Environment 39*(4), 385–397.

Chen, C., C.-H. Lin, Z. Long, and Q. Chen (2014, feb). Predicting transient particle transport in enclosed environments with the combined computational fluid dynamics and Markov chain method. *Indoor Air 24*(1), 81–92.

Chen, C., W. Liu, C.-H. Lin, and Q. Chen (2015a). A Markov chain model for predicting transient particle transport in enclosed environments. *Building and Environment 90*, 30–36.

Chen, C., W. Liu, C.-h. Lin, and Q. Chen (2015b). Comparing the Markov Chain Model with the Eulerian and Lagrangian Models for Indoor Transient Particle Transport Simulations. *Aerosol Science & Technology 49*(November), 857–871.

Chen, Y. L. and J. Wen (2008). Sensor system design for building indoor air protection. *Building and Environment 43*(7), 1278–1285.

Chvatal, V. (1979). A greedy heuristic for the set-covering problem. *Mathematics of operations research 4*(3), 233–235.

Demirev, P. A., A. B. Feldman, and J. S. Lin (2005). Chemical and biological Weapons: current concepts for Future Defenses. *Johns hopkins ApL TechnicAL DigesT 26*(4).

Du, Z., P. Xu, X. Jin, and Q. Liu (2015). Temperature sensor placement optimization for vav control using cfd–bes co-simulation strategy. *Building and Environment 85*, 104–113.

Duong, T. N. and S. E. Waldman (2016, sep). Importance of a Travel History in Evaluation of Respiratory Infections. *Current Emergency and Hospital Medicine Reports 4*(3), 141–152.

Fisk, W. J. and A. T. De Almeida (1998). Sensor-based demand-controlled ventilation: a review. *Energy and buildings 29*(1), 35–45.

Fontanini, A., U. Vaidya, A. Passalacqua, and B. Ganapathysubramanian (2017). Contaminant transport at large Courant numbers using Markov matrices. *Building and Environment 112*, 1–16.

Fontanini, A. D., U. Vaidya, and B. Ganapathysubramanian (2015, dec). Constructing Markov matrices for real-time transient contaminant transport analysis for indoor environments. *Building and Environment 94*, 68–81.

Fontanini, A. D., U. Vaidya, and B. Ganapathysubramanian (2016). A methodology for optimal placement of sensors in enclosed environments: A dynamical systems approach. *Building and Environment 100*, 145–161.

Herbstman, J. B., A. Sjödin, M. Kurzon, S. A. Lederman, R. S. Jones, V. Rauh, L. L. Needham, D. Tang, M. Niedzwiecki, R. Y. Wang, et al. (2015). Prenatal exposure to pbdes and neurodevelopment. *Everyday Environmental Toxins: Childrens Exposure Risks*, 223.

Jasak, H., A. Jemcov, and Z. Tukovi (2007). OpenFOAM: A C++ Library for Complex Physics Simulations. *International Workshop on Coupled Methods in Numerical Dynamics IUC*.

Kawashima, K., T. Matsumoto, and H. Akashi (2016). Disease Outbreaks: Critical Biological Factors and Control Strategies. pp. 173–204.

Kenyon, T. A., S. E. Valway, W. W. Ihle, I. M. Onorato, and K. G. Castro (1996, apr). Transmission of Multidrug-Resistant Mycobacterium tuberculosis during a Long Airplane Flight. *New England Journal of Medicine 334*(15), 933–938.

Li, F., J. Liu, J. Ren, X. Cao, and Y. Zhu (2016, may). Numerical investigation of airborne contaminant transport under different vortex structures in the aircraft cabin. *International Journal of Heat and Mass Transfer 96*, 287–295.

Liu, X. and Z. Zhai (2009a). Protecting a whole building from critical indoor contamination with optimal sensor network design and source identification methods. *Building and Environment 44*(11), 2276–2283.

Liu, X. and Z. J. Zhai (2009b). Prompt tracking of indoor airborne contaminant source location with probability-based inverse multi-zone modeling. *Building and Environment 44*(6), 1135–1143.

Lu, T., X. Lü, and M. Viljanen (2011). A novel and dynamic demand-controlled ventilation strategy for co 2 control and energy saving in buildings. *Energy and Buildings 43*(9), 2499–2508.

Mazumdar, S. and Q. Chen (2008). Influence of cabin conditions on placement and response of contaminant detection sensors in a commercial aircraft. *J. Environ. Monit. 10*(1), 71–81.

Namilae, S., A. Srinivasan, A. Mubayi, M. Scotch, and R. Pahle (2017, jan). Self-propelled pedestrian dynamics model: Application to passenger movement and infection propagation in airplanes. *Physica A: Statistical Mechanics and its Applications 465*, 248–260.

Nielsen, P., L. Rong, and I. Olmedo (1990). The iea annex 20 two-dimensional benchmark test for cfd predictions. *homes.civil.aau.dk*.

Olsen, S. J., H.-L. Chang, T. Y.-Y. Cheung, A. F.-Y. Tang, T. L. Fisk, S. P.-L. Ooi, H.-W. Kuo, D. D.-S. Jiang, K.-T. Chen, J. Lando, K.-H. Hsu, T.-J. Chen, and S. F. Dowell (2003, dec). Transmission of the Severe Acute Respiratory Syndrome on Aircraft. *New England Journal of Medicine 349*(25), 2416–2422.

Ostfield, M. L., R. Danzig, P. Berkowsky, R. A. Falkenrath, R. Preston, E. Gursky, T. Inglesby, T. O'Toole, A. Fauci, R. Preston, B. Durham, S. P. Layne, T. J. Beugelsdijk, M. J. Hall, A. E. Norwood, R. J. Ursano, C. S. Fullerton, C. F. Chyba, L. Garrett, M. Moodie, B. Kellman, J. Brower, P. Chalk, C. F. Chyba, R. S. Murch, W. J. Bicknell, K. D. Bloem, Brower, Chalk, Brower, Chalk, D. A. Ashford, R. M. Kaiser, M. E. Bales, K. Shutt, A. Patrawalla, A. McShan, J. W. Tappero, B. A. Perkins, A. L. Dannenberg, J. J. Hamre, and A. E. Smithson (2004). Bioterrorism as a Foreign Policy Issue. *SAIS Review 24*(1), 131–146.

Petzold, J., A. Pietzowski, F. Bagci, W. Trumler, and T. Ungerer (2005). Prediction of Indoor Movements Using Bayesian Networks. pp. 211–222. Springer Berlin Heidelberg.

Rajaram, R., U. Vaidya, M. Fardad, and B. Ganapathysubramanian (2010, aug). Stability in the almost everywhere sense: A linear transfer operator approach. *Journal of Mathematical Analysis and Applications 368*(1), 144–156.

Salmanzadeh, M., G. Zahedi, G. Ahmadi, D. Marr, and M. Glauser (2012). Computational modeling of effects of thermal plume adjacent to the body on

the indoor airflow and particle transport. *Journal of Aerosol Science 53*, 29–39.

Sarigiannis, D. A. (2013). The WHO Regional Office for Europe.

Stuart, A. L. and D. A. Wilkening (2005). Degradation of Biological Weapons Agents in the Environment: Implications for Terrorism Response.

Tham, K. W. (2016, oct). Indoor air quality and its effects on humansA review of challenges and developments in the last 30 years. *Energy and Buildings 130*, 637–650.

Vaidya, U., R. Rajaram, and S. Dasgupta (2012a). Actuator and sensor placement in linear advection PDE with building system application. *Journal of Mathematical Analysis and Applications 394*, 213–224.

Vaidya, U., R. Rajaram, and S. Dasgupta (2012b). Actuator and sensor placement in linear advection pde with building system application. *Journal of Mathematical Analysis and Applications 394*(1), 213–224.

Wenzel, R. P. (1996, apr). Airline Travel and Infection. *New England Journal of Medicine 334*(15), 981–982.

Zhang, T. and Q. Chen (2007, aug). Identification of contaminant sources in enclosed spaces by a single sensor. *Indoor Air 0*(0), 070901071522001–???

Zhou, L. and F. Haghighat (2009). Optimization of ventilation systems in office environment, part ii: Results and discussions. *Building and Environment 44*(4), 657–665.

Zhou, P., G. Huang, L. Zhang, and K.-F. Tsang (2015). Wireless sensor network based monitoring system for a large-scale indoor space: data process and supply air allocation optimization. *Energy and Buildings 103*, 365–374.

Zukowska, D., A. Melikov, and Z. Popiolek (2012). Impact of personal factors and furniture arrangement on the thermal plume above a sitting occupant. *Building and Environment 49*, 104–116.